Electron capture in collisions of N^{5+} ions with H atoms from the meV to keV energy regions

N. Shimakura* and M. Kimura
Argonne National Laboratory, Argonne, Illinois 60439
and Department of Physics, Rice University, Houston, Texas 77251
(Received 7 May 1990; revised manuscript received 1 February 1991)

Quantum-mechanical and semiclassical molecular-orbital expansion methods are employed to investigate a single-electron-capture mechanism in $N^{5+}+H$ collisions in the energy range from 10 meV/amu to 10 keV/amu. The dominant electron-capture channels in the entire regime are found to be $N^{4+}(4s)$, $N^{4+}(4p)$, and to some extent $N^{4+}(4d)$. The $N^{4+}(4f)$ channel is found to make small contributions at any energy because of its near diabaticity with respect to the initial channel. Agreement for total and n-shell captures with recent measurements is excellent in the entire energy regime, and agreement for l-shell capture with measurements is reasonable for most cases. Furthermore, several shape resonances due to rovibrational states of the transient quasimolecule are found below 1 eV, and a large, broad structure arising from trajectory effects due to the weak attractive polarization potential is found below 60 meV/amu. The origins of differences between the present results and the measurements and other theoretical calculations are also discussed.

I. INTRODUCTION

Theoretical and experimental studies of various processes in collisions of multiply charged ions with atoms have been a central focus of research on atomic collisions for the past decade. This is due in part to applications in areas of technology and in other subfields in physics [1]. However, the majority of experimental studies have been devoted to electron-capture processes within a relatively narrow energy region at higher energies (above the low-keV regime) [1]. Only recently have reports [2,3] appeared on electron capture in collisions of C^{5+}, N^{5+}, and O^{5+} ions with H atoms at energies below 100 eV/amu. These new low-energy measurements are important; combined with high-energy data, they provide a stringent test of the theory. Several theoretical attempts [4–7] have been made to study electron capture in N^{5+} + H collisions, but none of them systematically covers such a wide range of energy. General agreement of the total capture cross sections among theories and experiments previously reported within a narrow energy region is reasonably good.

As the first in a series of studies on electron capture in collisions of C^{5+}, N^{5+}, and O^{5+} ions with H atoms in the energy region 10 meV/amu to 10 keV/amu, this research on N^{5+} + H collisions has two principal objectives: (i) the reasonably accurate determination of both total and partial (n,l) cross sections over the entire energy region and (ii) the search for structures in the total cross section at low energy (below 1–2 eV), which have been attributed to "trajectory effects" [2,3] and shape resonances. As a theoretical tool for a study of the collision dynamics of the present study, a molecular-orbital expansion method within a fully quantum-mechanical representation for low energy (below 100 eV/amu) and a semiclassical representation for intermediate energy (above 100 eV/amu) with inclusion of atomic (plane-wave) electron translation factors up to first order in velocity is employed.

II. SUMMARY OF THEORY

A. Molecular states

The molecular electronic states are obtained by using a modified valence-bond configuration-interaction (CI) method with Gaussian-type pseudopotentials representing the N^{5+} core [8]. Hence only one active electron has been treated explicitly.

The form of the pseudopotential is

$$V(\mathbf{r})=\sum_{l,m} V_l(r)|Y_{lm}\rangle\langle Y_{lm}|$$

and

$$V_l(r)=A_l\exp(-\xi_l r^2)-\frac{\alpha_d}{2(r^2+d^2)^2}-\frac{\alpha_q}{2(r^2+d^2)^3}+\frac{5}{r}\ , \tag{1}$$

TABLE I. N^{5+} pseudopotential parameters.

Parameter	Value (a.u.)
A_0	54.555 325 339
A_1	−2.703 778 324 36
A_2	−0.472 270 196 513
ξ_0	9.682 625 759 99
ξ_1	10.998 562 837 5
ξ_2	7.014 003 190 62
d	0.227 279 7
α_d	0.004 63
α_q	0.000 38

TABLE II. Orbital exponents of the Slater-type orbital basis function.

N^{4+}		H	
Orbital	Exponent	Orbital	Exponent
2s	11.405	1s	2.0
	4.748		1.0
	2.677		0.5
2p	2.688	2s	0.5
	1.589	2p	1.0
3s	1.483 11		0.5
3p	1.637 96		
3d	1.670 70		
4s	1.324 59		
4p	1.150 19		
4d	1.139 94		
4f	1.253 77		
5s	1.715 02		
5p	2.172 48		
5d	2.875 64		
5f	1.365 72		

where $|Y_{lm}\rangle$ are the spherical harmonics. In Eq. (1), A_l and ξ_l are l-dependent parameters chosen to fit spectroscopic data. Values of the dipole and quadrupole polarizabilities α_q and α_q were taken from the review by Dalgarno [9]. The cutoff radius d was determined by a Hartree-Fock calculation. The pseudopotential parameters are given in Table I. In the CI calculation, Slater-type orbitals (STO's) were used to construct basis sets, consisting of 26 STOs for N^{4+} and 8 STO's for H. The orbital exponents for the N^{4+} ion were obtained by optimizing the energies of the ionic levels, while those of the H atom were taken from previous work by Sato *et al.* [10]. The Slater exponents used are given in Table II. The accuracy of the present molecular calculation with respect to the spectroscopic energies is better than 0.5% for all states.

B. Coupled equations

The following brief summary of the theory [11] used is based on the formal theory of slow ion-atom collisions extensively described by Delos [12].

1. Fully quantum-mechanical representation

By expanding the total scattering wave function in terms of products of electronic wave functions, nuclear (scattering) wave functions, and electron translation factors (ETF's), substituting the expansion into the Schrödinger equation, and expanding the ETF in powers of relative velocity v, to retain the terms up through order v, one obtains a set of second-order coupled equations for the nuclear radial functions $X^a(R)$ [11,12]:

$$\left[\frac{1}{2\mu}\left[-\nabla_R \underline{I}+(\underline{P}+\underline{A})\right]^2+\varepsilon-EI\right]\underline{X}^a(R)=0\ , \quad (2)$$

$$\underline{P}=\langle j|-i\nabla_R|i\rangle\ , \quad (3a)$$

$$\underline{A}=-\frac{i}{2}(\varepsilon_j-\varepsilon_i)\langle j|f_i(\mathbf{R},\mathbf{r})\mathbf{r}|i\rangle\ , \quad (3b)$$

where $\underline{P}$ and $\underline{A}$ represent the nonadiabatic coupling (matrix), and its ETF correction; E and $\underline{\varepsilon}$ represent total and adiabatic electronic energies; and μ is the reduced mass of the system. In Eqs. (3), $\varepsilon_j, |j\rangle$, and $f_i(\mathbf{R},\mathbf{r})$ describe the adiabatic energy of the jth state, its eigenfunction, and its switching function in the ETF [11]. It may be worthwhile noting that since our molecular states $|j\rangle$ are eigenfunctions of electronic Hamiltonian, additional small coupling terms appeared in an original coupled equations vanish, yielding a simplified Eq. (2). These $\underline{P}$ and $\underline{A}$ couplings can be divided into two contributions in the rotational frame coordinate, viz., radial and rotational couplings. In the present calculation, dominant couplings are important at large R and hence atomic (plane-wave) ETF's [11] are employed, i.e., $f_i(\mathbf{R},\mathbf{r})=\pm 1$, depending upon the atomic site. Introduction of the ETF in a quantum-mechanical formulation is not based on a rigorous treatment; a more general derivation without introducing the ETF explicitly can be found in Ref. [12].

It is numerically more tractable to treat Eq. (2) in a diabatic representation rather than in an adiabatic representation, thereby avoiding numerical problems due to the presence of sharp radial coupling. The transformation is achieved through a matrix $\underline{C}(R)$ [13], viz., $\underline{X}^d=\underline{C}^{-1}\underline{X}^a$ for the nuclear radial wave function and $\underline{V}^d=\underline{C}^{-1}\underline{\varepsilon}\,\underline{C}$ for the diabatic potential matrix. The matrix $\underline{C}(R)$ is determined numerically by solving

$$\frac{d\underline{C}}{dR}+(\underline{P}+\underline{A})\underline{C}=0\ , \quad (4)$$

where $\mathbf{C}$ satisfies the boundary condition

$$\lim_{R\to\infty}\underline{C}(R)=I\ . \quad (5)$$

In the diabatic representation, $\underline{X}^d$ satisfies

$$\left[\frac{1}{2\mu}\nabla_R^2\underline{I}-\underline{V}^d(R)+EI\right]\underline{X}^d(R)=0\ . \quad (6)$$

Equation (6) is then solved numerically for each partial wave by using the log-derivative method [14] to extract the scattering S matrix. From the S matrix for each partial wave, the differential cross section is obtained as

$$\frac{d\sigma}{d\Omega}=\frac{1}{4k^2}\left|\sum_l(2l+1)S^lP_l(\cos\theta)\right|^2\ , \quad (7)$$

where $k=\sqrt{2\mu E}$ and $P_l(x)$ represents the Legendre polynomial. Integration over all angles gives the total cross section.

2. Semiclassical representation

At higher collision energies, a semiclassical approach is valid. One conveniently starts with the time-dependent Schrödinger equation and assumes the heavy-particle velocity v. By expanding the total scattering wave function in terms of a product of time-dependent coefficients, electronic wave functions, and the ETF, substituting this expansion into the time-dependent Schrödinger equation,

and expanding the ETF in terms of v, one derives a set of first-order coupled equation [11]:

$$i\dot{a}_j=\varepsilon_j a_j+\sum_i \mathbf{v}\cdot(\underline{P}+\underline{A})_{ij}a_i \ , \tag{8}$$

where $\underline{P}$ and $\underline{A}$ represent, again, nonadiabatic coupling (matrices) and the ETF correction (to the first order in v), respectively, as given in Eqs. (3). A classical trajectory for the heavy-particle motion is assumed. Equation (8) is then solved numerically subject to the initial conditions $a_i\ (t\rightarrow-\infty)=\delta_{ij}$. The transition probability to the mth state, defined as a function of impact energy E and impact parameter b at $t\rightarrow+\infty$, is

$$P_m(E,b)=|a_m(E,b)|^2 \ , \tag{9}$$

and the total cross section for excitation of the mth state is given by

$$\sigma_m(E)=2\pi\int db\ bP_m(E,b) \ . \tag{10}$$

III. RESULTS

A. Adiabatic potential energies and coupling matrix elements

The potential energies of the NH^{5+} system are presented in Fig. 1, and an expanded scale of the outer crossing region is given in Fig. 2. These figures indicate that the N^{4+} ($n=4$) states dominate the electron-capture processes at low to intermediate energies and suggest that, because of large energy defects, only at high impact energies do the N^{4+} ($n=3$) states contribute to electron capture. Two important avoided crossings can be seen at about $11.75a_0$ ($=R_1$) between the 4Σ and 5Σ states and around $13.29a_0$ ($=R_2$) between the 5Σ and 6Σ states, with energy splittings of about 0.008 and 0.002 a.u., respectively. Although crossings between the 6Σ and 7Σ states at $R=14.11a_0$ ($=R_3$) and the 7Σ and 8Σ states at $14.70a_0$ ($=R_4$) are seen in Fig. 1, the corresponding energy splittings are extremely small, with values less than 10^{-5} and 10^{-6} a.u., respectively; hence these crossings are considered to be near diabatic in nature in the actual dynamics and we treat them accordingly.

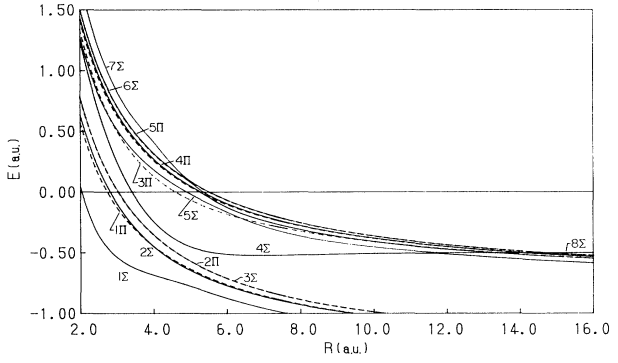

FIG. 1. Adiabatic potentials of the NH^{5+} system. Solid and dashed curves represent Σ and Π states, respectively. 1Σ, 2Σ, 3Σ, 4Σ, 5Σ, 6Σ, 7Σ, 8Σ, 1Π, 2Π, 3Π, 4Π, and 5Π correspond to $N^{4+}(3s)$, $N^{4+}(3p)$, $N^{4+}(3d)$, $N^{4+}(4s)$, $N^{4+}(4p)$, $N^{4+}(4d)$, $N^{4+}(4f)$, $N^{5+}+H$, $N^{4+}(3p)$, $N^{4+}(3d)$, $N^{4+}(4p)$, $N^{4+}(4d)$, and $N^{4+}(4f)$.

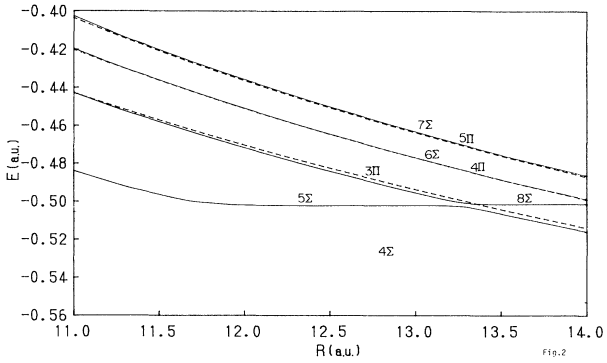

FIG. 2. Adiabatic potentials in the region of strong avoided crossings between N^{4+} ($n=4$) and H. Symbols are as in Fig. 1.

The values of the radial couplings between 4Σ and 5Σ states and between the 5Σ and 8Σ states are displayed in Fig. 3. Shipsey, Browne, and Olson[4] showed an additional peak in the radial coupling between the 4Σ and 5Σ states at around $R=8$ a.u. but no such a peak is observed in our results. Gargaud and McCarroll[5] noted that such a peak may appear, depending on the origin of the electron coordinates chosen, and the additional peak found by Shipsey, Browne, and Olson[4] may be due to this artifact. The half-widths of the peaks of the radial couplings between the 4Σ and 5Σ states at R_1 and between the 5Σ and 8Σ states at R_2 are 0.52 and 0.18 a.u. (see Fig. 2), which may suggest a stronger diabatic nature in the crossing at R_2 than at R_1. On the other hand, the half-widths of the radial couplings between the 6Σ and 8Σ states at R_3 and between the 7Σ and 8Σ states at R_4 are less than 2×10^{-4} and 1×10^{-4} a.u. (see Fig. 2), these values clearly support the argument for diabaticity of the

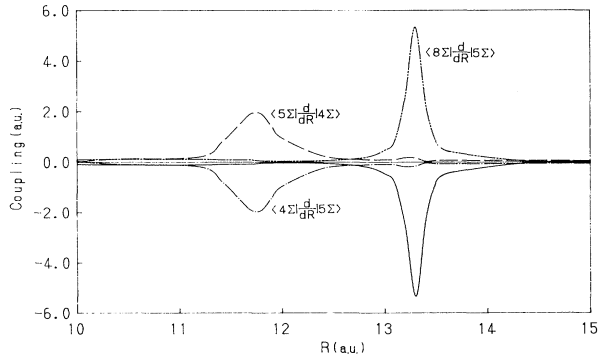

FIG. 3. Representative radial couplings between 4Σ and 5Σ states and 5Σ and 8Σ states.

crossings between 6Σ, 7Σ, and 8Σ discussed above. The radial couplings among different n manifolds are generally weak, suggesting little flux exchange among these manifolds. Contributions from rotational couplings are of secondary importance for the flux exit, but they play a crucial role for the flux redistribution within given n manifolds: These rotational couplings are included in the calculations for electron capture.

B. Transition probabilities

1. *High-energy ($E \geq 100$ eV) semiclassical results*

A 13-channel close-coupling calculation was performed to obtain the electron-capture probability in the energy range from 0.04 to 10 keV/amu. In this calculation, all eight Σ states and five Π states arising from the N^{4+} ($n=4$ and 3) manifolds, plus the initial $N^{5+}+H$ channel as shown in Fig. 1, were included. The time-evolution study of the transition probabilities (see below) clearly shows that some parts of the flux are transferred to electron-capture channels on *the incoming part of the collision*. This transferred flux begins its redistribution among other capture channels soon after the transition on trajectories different from the initial trajectory. In addition, several articles in the literature have reported cross sections resulting from collisions of multiply charged ions with atoms at low energy, made by using a repulsive Coulomb trajectory without much testing. Hence we felt it interesting to examine the trajectory effect on the transition probabilities for a wide range of energies by using two quite opposite trajectories. We used both straight-line and repulsive Coulomb (of the exit channel) trajectories for the heavy-particle motion. Values of total probabilities times impact parameters obtained by (i) a straight-line trajectory and (ii) a Coulomb trajectory are plotted as functions of impact parameter in Figs. 4 and 5 for $v=0.05$ and 0.15 a.u., respectively. Several features are noteworthy.

(a) The transition probabilities at these two velocities are significant only in the region of $b \leq 12a_0$, reflecting the dominance of the curve crossing at R_1. This observation is generally valid at other velocities.

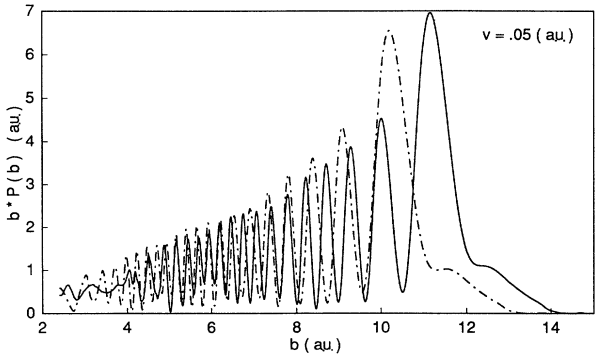

FIG. 4. Total transition probability by the semiclassical method at $v=0.05$ a.u. Solid line, a straight-line trajectory; dot-dashed line, a Coulomb trajectory.

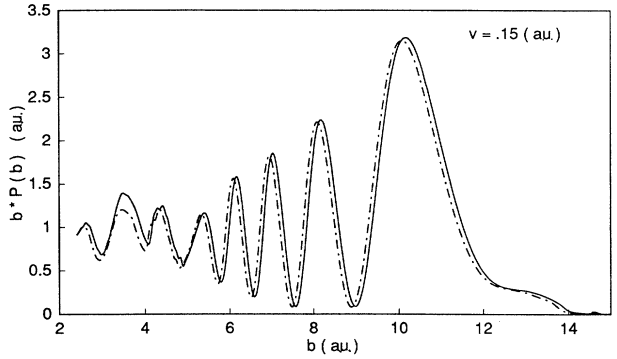

FIG. 5. Total transition probability by the semiclassical method at $v=0.15$ a.u. Solid line, a straight-line trajectory; dash-dot line, a Coulomb trajectory.

(b) A trajectory effect becomes weak as the energy increases, making probabilities for the straight-line and Coulomb trajectories become nearly identical at higher velocities.

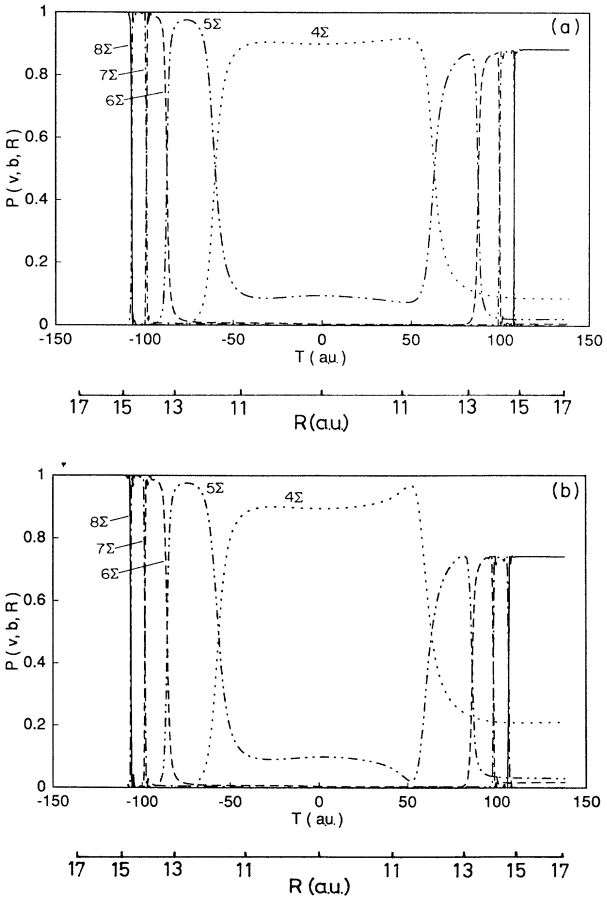

FIG. 6. Collision histories of probabilities at $v=0.1$ a.u. and $b=10a_0$ for (a) a straight-line trajectory and (b), a Coulomb trajectory.

(c) The peaks in the oscillations of the probabilities for the Coulomb trajectory are shifted to smaller b compared to those for the straight-line case because of the stronger repulsion in the former case; this phenomenon was pointed out by Knudson and Thorson [15].

(d) The position of the largest peak shifts to larger impact parameter as the energy decreases.

(e) The number of oscillations in the probability drastically increases as the energy is decreased, reflecting the increased interaction time for electron transfer in the slower collision.

The collision histories (i.e., the time evolutions of the transition probabilities) for several dominant channels are plotted as a function of time (and R) in case of $v=0.1$ a.u. and $b=10a_0$ for straight-line and Coulomb trajectories in Figs. 6(a) and 6(b), respectively. Under these conditions, the transition probabilities of the 1Σ, 2Σ, 3Σ, and all Π states are negligible. The transition probabilities from the initial channel to 7Σ and 6Σ have a value of nearly 1 at each corresponding crossing. That from 6Σ to 5Σ [$N^{4+}(4p)$] has a value of 0.95 at R_2 ($13.29a_0$); hence this transition is also regarded as near diabatic. Most of the flux is transferred from 6Σ to 5Σ and then to 4Σ on the incoming part of the collision trajectory, but it is transferred back from 4Σ to 5Σ and then to 6Σ and 7Σ on the outgoing part of the trajectory because the collision partners twice pass through these reaction windows around R_2 and R_3. Comparing Figs. 6(a) and 6(b) reveals that the transition probabilities are nearly identical on the incoming part of the trajectory for both the straight-line and Coulomb trajectories. The Coulomb effect appears on the outgoing trajectory of the collision, particularly after R_1. This feature is obvious from the nature of the trajectories.

2. *Low-energy ($E<100$ eV) quantum results*

Two- and three-state quantum-mechanical close-coupling calculations were performed for the lower collision energies with the initial states 4Σ $N^{4+}(4s)$ and 5Σ $N^{4+}(4p)$. (In adiabatic notation, this corresponds to 6Σ, 7Σ, and 8Σ at $R\le R_3$, $R_3<R<R_4$, and $R\ge R_4$, respectively.) Squares of the scattering S-matrix element corresponding to charge transfer are displayed as a function of partial wave l for several energies in Fig. 7. Comparing the S matrix of $E=0.1$ eV with that of $E=0.15$ eV indicates that a large contribution from $l\ge 18$ occurs for the latter. This contribution is caused by a transient rovibrational state (a shape resonance) of the quasimolecule formed during a collision. A detailed discussion of the resonance is deferred to Sec. III D.

C. Cross sections

Figure 8 displays the total cross sections from the present work along with measurements [3,16–20] and other calculations [4–6]. The overall agreement of the present results with all the measurements is excellent over the entire energy region studied. Our semiclassical cross sections lie about 25% lower than the recent measurement by Huq, Havener, and Phaneuf [3] at impact

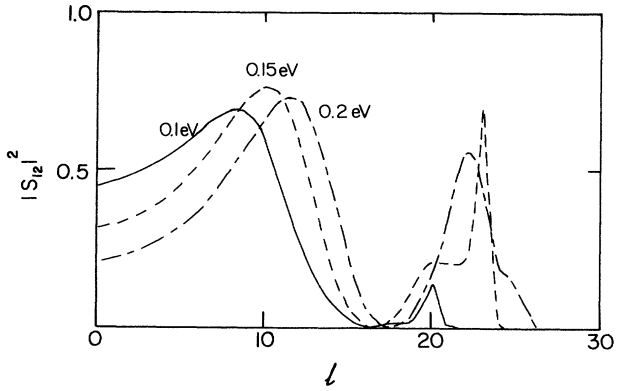

FIG. 7. Squares of the scattering S-matrix element vs partial wave at $E=0.1$, 0.15, and 0.2 eV. A large contribution from $l\ge 18$ at $E=0.15$ eV is due to a shape resonance.

energies below 0.2 keV/amu, while in the region of $E=1$ eV/amu to 0.2 keV/amu, the agreement of our quantum results with the data by Huq, Havener, and Phaneuf [3] is excellent. The energy dependence of our results compares very well with all the measurements.

1. *Comparison with theories*

Four theoretical studies of the present process exist for the *total* cross section. Shipsey, Browne, and Olson [4] calculated the cross sections in the energy range from 0.01 to 100 keV/amu by using a semiclassical molecular-orbital (MO) method *without* the ETF's below 6 keV/amu. The molecular states were obtained by means of a three-electron, valence-bond CI method. The positions and energy splittings at the sharp avoided crossings among the 4Σ–8Σ states are nearly identical to ours. Shipsey, Browne, and Olson carried out five-channel close-coupling calculations including 3Σ, 4Σ, 5Σ, 2Π, and 3Π with a straight-line trajectory. As is clear from our larger MO calculation, inclusion of the contribution from 6Σ appears to be necessary for the correct description of the collision dynamics.

Hanssen *et al.* [6] calculated the cross section in the energy range from 0.3 to 30 keV/amu by using a semiclassical MO method. The molecular states were obtained by a model potential method. The precision of their potentials seems to be comparable to that of the present results. Hanssen *et al.* carried out four- and nine-channel close-coupling calculations with a straight-line trajectory with the 4Σ, 5Σ, 3Π, and 8Σ (initial) states plus additional states from the N^{4+} ($n=3$) manifold. State-independent ETF's were implemented in the calculation. Their results lie about 12% higher than ours from 0.3 to 4 keV/amu, and the agreement becomes less satisfactory at 10 keV/amu, with their result being 25% larger. We find that the 6Σ [$N^{4+}(4d)$] and 7Σ [$N^{4+}(4f)$] states become increasingly important in our calculation, amounting to 24% of the total as the energy is increased above 2 keV/amu; thus we conclude that these states should be included in the calculations.

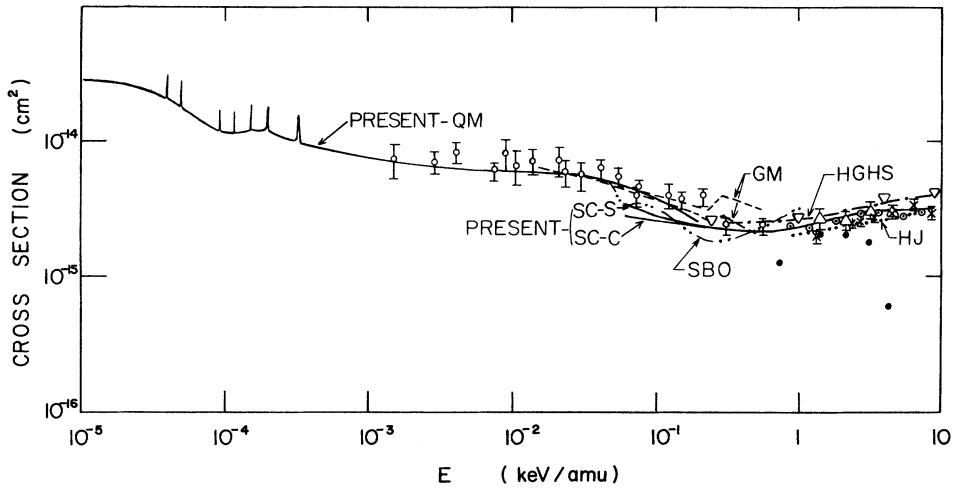

FIG. 8. Total electron-capture cross section. Theory: solid line, present-QM, quantum mechanical; SC-C, Coulomb trajectory; SC-S, straight-line trajectory; —●— (HGHS), Ref. [6]; — — —, (GM), Ref. [5]; -●●- (SBO), Ref. [4]; . . . (HJ), Ref. [7]. Experiment: ○ Ref. [3]; ●, Ref. [18]; ×, Ref. [16], Δ, Ref. [17]; ∇, Ref. [19]; ⊙, Ref. [20].

Hence reasonably good agreement between our results and those of Hanssen *et al.* may be regarded in part as fortuitous.

Gargaud and McCarroll [5] applied a quantum-mechanical MO method for electron capture in the energy range from 1 eV/amu to 5 keV/amu. Their molecular states were obtained by a model potential method, and a five-channel close-coupling calculation with 1Σ, 2Σ, 3Σ, 4Σ, and 8Σ states was carried out *without* the ETF's. Because they neglected the ETF's, their cross sections varied by about 65% at 0.45 keV/amu, depending on the origin of the electron coordinates they chose, although the cross sections do appear to converge at lower energies below 40 eV/amu. However, their cross sections below 50 eV/amu seem to increase linearly with decreasing energy, while the present quantum results are rather flat between 20 and 60 eV/amu. The experimental data of Huq, Havener, and Phaneuf [3] also seem to display flatness in this energy region, resembling the present result. Above 0.3 keV/amu, the results of Gargaud and McCarroll [5] show a sharp drop in the cross section, which does not agree with any experiments or theories.

Harel and Jouin [7] employed a semiclassical MO method (with a straight-line trajectory) to calculate $n=3$ and 4 partial cross sections in the energy range from 0.9 to 7.3 keV/amu. The molecular states were obtained by a model potential method, and all states correlating to N^{4+} ($n=3$ and 4) manifolds were included as in the present calculation. State-independent, parametrized ETF's were also included in the calculation. Their $n=4$ partial cross section is nearly identical with ours below 1.5 keV/amu, but their result begins to deviate from ours above this energy, with theirs being about 25% larger at 7.3 keV/amu. A closer examination of the l population in the $n=4$ manifold partial cross section reveals that their N^{4+} ($4d$ and $4f$) distributions constitute about 84% of the total at 7.3 keV/amu, while N^{4+} ($4p$ and $4d$) distributions amount to about 74% in the present result. Hence the difference in prediction of l population between the two calculations appears to be significant. Considering the very small energy splitting between the initial:8Σ and $N^{4+}(4f)$:7Σ states at $R=14.7a_0$ crossing (which we regard as strongly diabatic in character, as discussed in Sec. III A), it is somewhat puzzling to observe such a large contribution of the $N^{4+}(4f)$ state in this energy region. This rather sharply increasing trend of the $N^{4+}(4f)$ state population above 2 keV/amu in the calculation by Harel and Jouin is responsible for the discrepancy in the total between the two calculations. This difference could be attributable in part to different treatment of the ETF.

In the energy region above 50 eV, there are some variations among the various calculations.

Next, we will discuss the effect of two trajectories in our results. At lower energies, below a hundred eV, the cross sections using the Coulomb trajectory are as much as 18% smaller than the straight-line cross sections. This reduction of the Coulomb trajectory cross section comes from smaller contribution from states that couple at the inner R region because the strong Coulomb repulsion prevents the colliding partners from approaching close enough to make those couplings effective. However, with increasing impact energies, the results for different trajectories converge. They eventually agree above 1 keV/amu; Figs. 4 and 5 show that at $E=0.06$ and 0.56 keV/amu (or $v=0.05$ and 0.15 a.u.), the percentage differences are about 18.0% and 1.0%, respectively. Differences seen in the quantum and semiclassical results at $E<100$ eV are due partly to the different sizes of the basis sets used and the uncertainties of trajectories used in the semiclassical calculation.

2. *Comparison with measurements*

Here we discuss in detail the comparison with measurements above 0.5 keV/amu. In this energy region, the results from the two different trajectories are identical. The present l-shell cross sections are displayed in Fig. 9 along with the measurements by Dijkkamp *et al.* [20]. Our results clearly show that at the higher impact energies, above 1 keV/amu, the electron-capture process occurs predominantly through the $4p$, $4d$, and $4s$ state populations of the $n=4$ manifold and the $3p$ state population of the $n=3$ manifold of the N^{4+} ion. A small, but non-negligible, contribution from other $n=3$ manifolds is also found. However, at the intermediate energies, below 0.5 keV/amu, only the $4s$ and $4p$ (and, to a smaller extent, $4d$) states of the N^{4+} ion are important. At lower energies, below 0.2 keV/amu, the dominant state is not the $4p$ state but the $4s$ state, and as the energy increases, the situation reverses. This is because the energy splitting and corresponding coupling between the 4Σ and 5Σ states at R_1 still make this crossing diabatic. The agreement between our results and the measurements by Dijkkamp *et al.* [20] is reasonable for the 4s and 4d states. However, the difference of the partial cross sections for the $4p$ and $4f$ states is especially noticeable. Possible sources of errors in our calculation are the (i) trajectory effect, which may contribute to the flux redistribution $(n,l$ distribution), (ii) numerical uncertainty in evaluating the radial coupling matrix elements at two outer crossings, and (iii) the choice of ETF's. We estimate our total error arising from these uncertainties less than 20%. As we will see next, our results for n distribution agree very well in magnitude and energy dependence with the measurement by Dijkkaamp *et al.* [20]. Hence we suspect that inaccuracy in the experiment by Dijkkamp *et al.* [20] is partly responsible for the disagreement in the $4p$ and $4f$ populations.

Figure 10 compares the present n-shell cross sections

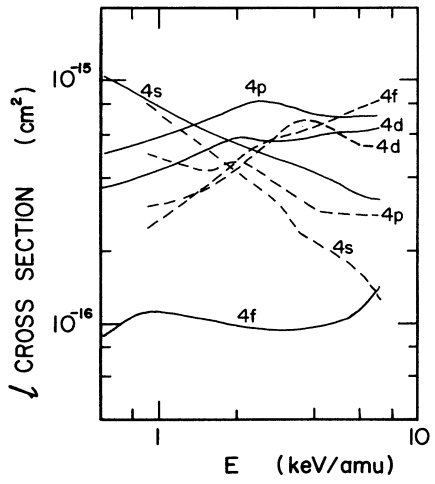

FIG. 9. Partial l-shell cross sections: ——, present results; — — —, Dijkkamp *et al.* [20].

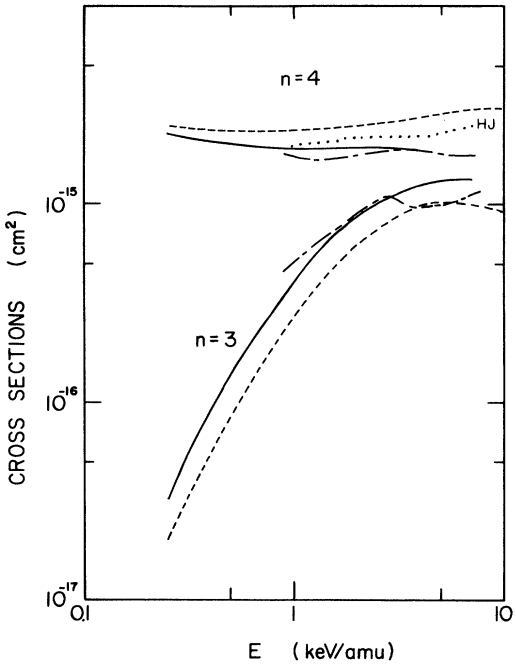

FIG. 10. Partial n-shell cross sections: ——, present results; (HJ) . . . ., [7]; — — —, Bendahman *et al.* [19]; —·—·—, Dijkkamp *et al.* [20].

(the sum of all l contributions) with the theory of Harel and Jouin [7] and measurements of Bendahman *et al.* [19] and Dijkkamp *et al.* [20]. Our results for the $n=3$ manifold are in excellent accord with those of Dijkkamp *et al.* below 3 keV/amu. Above this energy, the experiment by Dijkkamp *et al.* shows a dip at $E=4$ keV, then a slight increase at higher energies. In contrast, our results monotonically increase above 3 keV/amu. The result of Bendahman *et al.* shows similar energy dependence to ours, but it is smaller in magnitude, by approximately 25%.

In contrast, our results for the $n=4$ manifold are in excellent accord with those of Dijkkamp *et al.* above 3 keV/amu. Below this energy, the degree of the agreement is still reasonable, within 13%. The result of Dijkkamp *et al.* has a shallow minimum at $E=1.2$ keV/amu, while the structure in the present result is much weaker. The result of Bendahman *et al.* below 2 keV/amu shows an energy dependence similar to ours. However, their result has a slightly increasing trend above 2.5 keV/amu that is opposite to ours and that of Dijkkamp *et al.* In energy dependence, the theoretical result of Harel and Jouin [7] for the $n=4$ manifold is quite similar to the result of Bendahman *et al.* However, in magnitude the result of Harel and Jouin is consistently smaller (about 17%) than that of Bendahman *et al.*

D. Shape resonances and other structures

We found several resonances in the cross section below $E \leq 0.5$ eV that are due to rovibrational states of the

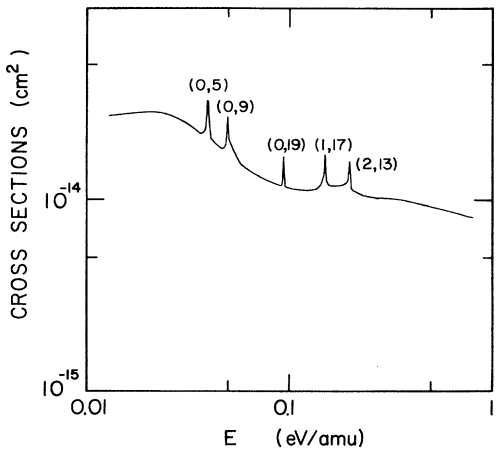

FIG. 11. Low-energy electron capture cross section. Resonances are labeled by (v,j), where v and J are the vibrational and rotational quantum numbers, respectively.

transient molecular ion. Assignments of vibrational v and rotational J states in the resonance around 50 meV $\leq E \leq 0.2$ eV are shown in Fig. 11. Most of these levels are low vibrational states with rather high rotational quantum numbers. This observation is not surprising because the shallow well in the 4Σ adiabatic potential can support only low vibrational states. Similar resonances have been observed in $He^+ + H$ collisions [21] and $N^{3+} + H$ collisions [22]. It is also apparent in Fig. 11 that the cross sections above and below 0.1 eV show different energy dependences. To determine the origin of this feature, we carried out some test calculations by artificially changing the potential well of the 4Σ state (the polarization potential). When the well is weakened, the magnitude of the cross section below 0.1 eV/amu decreases, and some resonances disappear. The situation reverses when the potential is strengthened. This observation suggests that the structure or change of slope in the cross section seen below 0.1 eV/amu is due to the polarization potential of the 4Σ state.

IV. CONCLUDING REMARKS

Electron-capture cross sections have been obtained by applying quantum-mechanical (3-channel) and semiclassical (13-channel) MO methods with inclusion of the atomic ETF's in the energy range from 10 meV/amu to 10 keV/amu. Although the total cross sections are relatively insensitive to collision energy, a shallow, broad minimum is found in the region of $E = 0.1-1$ keV/amu. As the energy decreases, the cross sections gently increase. Several shape resonances are found below 1 eV, and a large broad structure is apparent below 60 meV/amu.

At intermediate energies where the semiclassical method was applied, we observed appreciable differences between the cross sections obtained by employing straight-line and repulsive Coulomb trajectories, as expected, but these results converge with increasing energy above 0.15 keV/amu.

The dominant states of electron capture are the $4p$, $4d$, and $4s$ states at any energy studied, but at higher energies, above 0.4 keV/amu, the major contributors to electron capture are the $4s$, $4p$, $4d$, and $3p$ states.

ACKNOWLEDGMENTS

The authors thank Dr. N. F. Lane and Dr. W. Fritsch for useful discussions and comments. This work was supported in part by the U.S. Department of Energy, Assistant Secretary for Energy Research, Office of Health and Environmental Research, under Contract No. W-31-109-ENG-38 (M.K.); by Office of Basic Energy Science, Division of Chemical Sciences, through Rice University (N.S.); and by the R. A. Welch Foundation (N.S.). N. S. was also supported by a Grant-in-Aid for Scientific Research from the Ministry of Education of Japan (01540312). Some portions of the present calculation were carried out at the computer centers of Tohoku University and Niigata University. The travel grant was provided by a Grant-in-Aid for Scientific Research from the Ministry of Education of Japan (63044021).

*Permanent address: Chemistry Department, Division of General Education, Niigata University, Niigata, Japan.

[1] See, for example, review articles on recent progress in the field: R. K. Janev, L. P. Presnyakov, and V. P. Shevelko, *Physics of Highly Charged Ions* (Springer-Verlag, Berlin, 1985).
[2] C. C. Havener, M. S. Huq, N. F. Krause, P. A. Schulz, and R. A. Phaneuf, Phys. Rev. A **39**, 1725 (1989).
[3] M. S. Huq, C. C. Havener, and R. A. Phaneuf, Phys. Rev. A **40**, 1811 (1989).
[4] E. J. Shipsey, J. C. Browne, and R. E. Olson, J. Phys. B **14**, 869 (1981).
[5] M. Gargaud and R. McCarroll, J. Phys. B **18**, 463 (1985).
[6] J. Hanssen, R. Gayet, C. Harel, and A. Salin, J. Phys. B **17**, L323 (1984).
[7] C. Harel and H. Jouin, J. Phys. B **21**, 859 (1988).
[8] J. N. Bardsley, Case Stud. At. Phys. **4**, 299 (1974).
[9] A. Dalgarno, Adv. Phys. **11**, 281 (1962).
[10] H. Sato, M. Kimura, A. Wetmore, and R. E. Olson, J. Phys. B **16**, 3037 (1983).
[11] M. Kimura and N. F. Lane, in *Advances in Atomic, Molecular, and Optical Physics,* edited by D. R. Bates and B. Bederson (Academic, New York, 1989), Vol. 26, p. 79.
[12] J. B. Delos, Rev. Mod. Phys. **53**, 287 (1981).
[13] T. G. Heil, S. E. Butler, and A. Dalgarno, Phys. Rev. A **23**, 1100 (1981).
[14] B. R. Johnson, J. Comput. Phys. **13**, 445 (1973).
[15] S. K. Knudson and W. R. Thorson, Can. J. Phys. **48**, 313

(1970).
[16] D. H. Crandall, R. A. Phaneuf, and F. W. Meyer, Phys. Rev. A **19**, 504 (1979).
[17] W. Seim, A. Muller, I. Wirkner-Bott, and E. Salzborn, J. Phys. B **14**, 3475 (1981).
[18] M. N. Panov, A. A. Basalaev, and K. O. Lozhkin, Phys. Scr. T **3**, 124 (1983).
[19] M. Bendahman, S. Bliman, S. Dousson, D. Hitz, R. Gayet, J. Hanssen, C. Harel, and A. Salin, J. Phys. (Paris) **46**, 561 (1985).
[20] D. Dijkkamp, D. Circle, E. Vlieg, A. de Boer, and F. J. de Heer, J. Phys. B **18**, 4763 (1985).
[21] B. Zygelman, A. Dalgarno, M. Kimura, and N. F. Lane, Phys. Rev. A **40**, 2340 (1989).
[22] M. Rittby, N. Elander, E. Brandas, and A. Barany, J. Phys. B **17**, L677 (1984).